Type of the Paper (Article)

Estimates of the leaf area index using unmanned aerial vehicle images of an urban mangrove in the Vitória Bay, Brazil

Elizabeth Dell'Orto e Silva [1*], Alexandre Candido Xavier [2], Angélica Nogueira de Souza Tedesco[3], Aurélio Azevedo Barreto Neto[3], Luiz Eduardo Martins de Lima[3], José Eduardo Macedo Pezzopane[2], and Mônica Maria Pereira Tognella[1].

[1]Postgraduate Program in Oceanography, Federal University of Espírito Santo, Espírito Santo, Brazil; lisadellorto@gmail.com; monica.tognella@gmail.com

[2]Department of Forestry and Wood Sciences, Federal University of Espírito Santo, Espírito Santo, Brazil; alexandre.candido.xavier.ufes@gmail.com; pezzopane2007@yahoo.com.br

[3]Federal Institute of Espírito Santo, Espírito Santo, Brazil; aurelio@ifes.edu.br; angelica.nst@gmail.com; luisedu@ifes.edu.br

* Correspondence: lisadellorto@gmail.com; Tel.: +55-27-9922-60495

Abstract: The urban mangrove of the Vitória Bay, Espírito Santo, Southern Brazil suffers from anthropogenic impacts, which interfere in the foliar spectral response of its species. Identifying the spectral behavior of these species and creating regression models to indirectly obtain structure data like the Leaf Area Index (LAI) are powerful environmental monitoring tools. In this study, LAI was obtained in 32 plots distributed in four stations. In situ LAI regression analysis with the SAVI resulted in significant positive relationships (r^2 = 0.58). Forest variability regarding the degree of maturity and structural heterogeneity and LAI influenced the adjustment of vegetation indices (VIs). The highest regression values were obtained for the homogeneous field data, represented by *R. mangle* plots, which also had higher LAI values. The same field data were correlated with SAVI of a *RapidEye* image for comparison purposes. The results showed that, images obtained by a UAV have higher spatial resolution than the *Rapideye* image, and therefore had a greater influence of the background. Another point is that the statistical analysis of the field data with the IVs obtained from the *RapidEye* image did not present high regression coefficient (r^2 = 0.7), suggesting that the use of VIs applied to the study of urban mangroves needs to be better evaluated, observing the factors that influence the leaf spectral response.

Keywords: UAV images; mangrove; vegetation indices; Leaf Area Index (LAI)

1. Introduction

The Leaf Area Index (LAI) is defined as the total leaf area projected per area unit of land (m^2/m^2) [1]. This index allows calculations based on plant biomass and characterization of the canopy architecture, two structural parameters that provide information on the vigor of the vegetation cover. These estimates enable evaluating the physiognomic and physiological conditions of the canopies, as well as quantitative and qualitative analyses of energy and matter flows [2].

 doi:10.20944/preprints201810.0617.v1

Remote sensing studies using orbital sensors established relationships between vegetation indices (VIs) and LAI [3–5], as well as other biophysical information like biomass, canopy density [6–8], and species distribution [9,10].

LAI estimates using remote sensing techniques are affected by the soil type and shade, which may distort the results, usually resulting in decreased reflected radiance [11]. Besides, factors that can affect the spectral behavior of a vegetation canopy include the type of vegetation cover; orientation and spacing of trees; canopy morphology; internal structure of canopy elements; tree crown diameter; tree height; water content of plant and soil; plant health conditions; zenith and azimuth solar angles; latitude; and resolution of the equipment used [12].

The Soil-Adjusted Vegetation Index (SAVI) seeks to mitigate the effects of soil background. It was proposed based on studies carried out under different conditions of soil and vegetation cover (Huete 1988), as:

$$SAVI = \frac{(1+L)(\rho_{IV}-\rho_V)}{(L+\rho_{IV}+\rho_V)},$$

where ϱ_{IV} and ϱ_V are the reflectances of bands 4 and 3 of the Landsat 5 satellite, and L can vary from 0.1 to 0.5 according to characteristics of the analyzed canopy.

SAVI is based on the principle that the vegetation curve tends to approach the soil curve for low vegetation densities but varies the spectral responses in medium vegetation densities until there is almost no soil influence on high vegetation densities [13]. The SAVI equation is similar to that of the Normalized Difference Vegetation Index (NDVI) [14] plus a constant, L, which varies from 0 to 1 according to the degree of greater or lesser soil coverage, respectively. Likewise, there are three other modifications of the SAVI, the Transformed SAVI (TSAVI) [15,16], Modified SAVI (MSAVI) [17], and Optimized SAVI (OSAVI) [18].

Zhang et al. [19] discussed that, with the advent of hyperspectral sensors, other spectral indices had been developed. These include the Pigment Simple Ratio (PSR), which analyzes photosynthetic pigments and the Structure Insensitive Pigment Index (SIPI), which examines the structure and water content.

Working with VIs also requires radiometric calibration. Calibration is the process of transforming the digital number (DN) of each image pixel into values of physical parameters like radiance or reflectance [20].

The reflectance of a target can be described as a function of the wavelength and the directions of irradiation and observation, thus named Bidirectional Reflectance Distribution Function (BRDF) [21]. The BRDF correction process takes into account the changes of the energy recorded in the images caused by differences in geometry and instantaneous image acquisition, the anisotropy of the targets, information on solar and sensor angles, and shared points in images [22].

In the radiometric calibration of aerial photographs obtained with unmanned aerial vehicles (UAVs), the process is carried out for each photo, and not for the whole scene as for the orbital images. Variations in the Global Navigation Satellite System (GNSS) and UAV inertial systems can produce variations of the zenith angle (θv). According to [23], it is impossible to conduct directional measurements of canopies in the laboratory, and it is complicated to implement directional reflectance measurements in the open air. However, digital aerial photos, when taken with high frontal and lateral overlap, provide a convenient tool for analyzing the effects of directional reflectance.

Several authors have found positive correlations between LAI estimates collected in the field and VIs (e.g., NDVI) derived from satellite images [3,24], suggesting that highly accurate LAI thematic maps can be repeatedly derived from these sensors in considerable areas without the need for a high number of ground measurements. Most studies have been conducted in well-developed mangrove forests and, consequently, the robustness of such relationships in less ideal conditions, i.e., in plots of urban mangroves, also needs to be studied [25].

Therefore, this study aimed to test the feasibility of using a UAV to extract information from the structure of the mangrove trees of the Vitória Bay, Espírito Santo State, Southeastern Brazil.

Preprints (www.preprints.org) | NOT PEER-REVIEWED | Posted: 26 October 2018 doi:10.20944/preprints201810.0617.v1

Correlation analysis was performed between the data collected *in situ* (LAI, diameter at breast height (DBH), tree height, and density of individuals) and VIs (NDVI, SAVI) from images taken by a UAV. VIs were also calculated using a *Rapideye* satellite image, and the correlation analysis was performed with the same field data to compare the results.

The results showed that, even for the satellite images, the correlation analysis did not have a high coefficient of determination (r^2), suggesting that forest variability regarding the degree of maturity and structural heterogeneity and LAI influenced VIs adjustment. The highest regression values were obtained for the SAVI image with the most homogeneous field data, represented by *R. mangle plots*, which also had higher LAI values.

2. Materials and Methods

Four study areas were defined in the mangrove of the Vitória Bay, which extends through the municipalities of Vila Velha, Cariacica, Serra, and Vitória. The delimited areas are located in the municipality of Cariacica, with ~ 15 ha each (Figure 1). For each study area, there were eight field plots, totaling 32. The criteria for choosing these areas considered the localization of the Vitória airport and suitable places for takeoff and landing of the UAV.

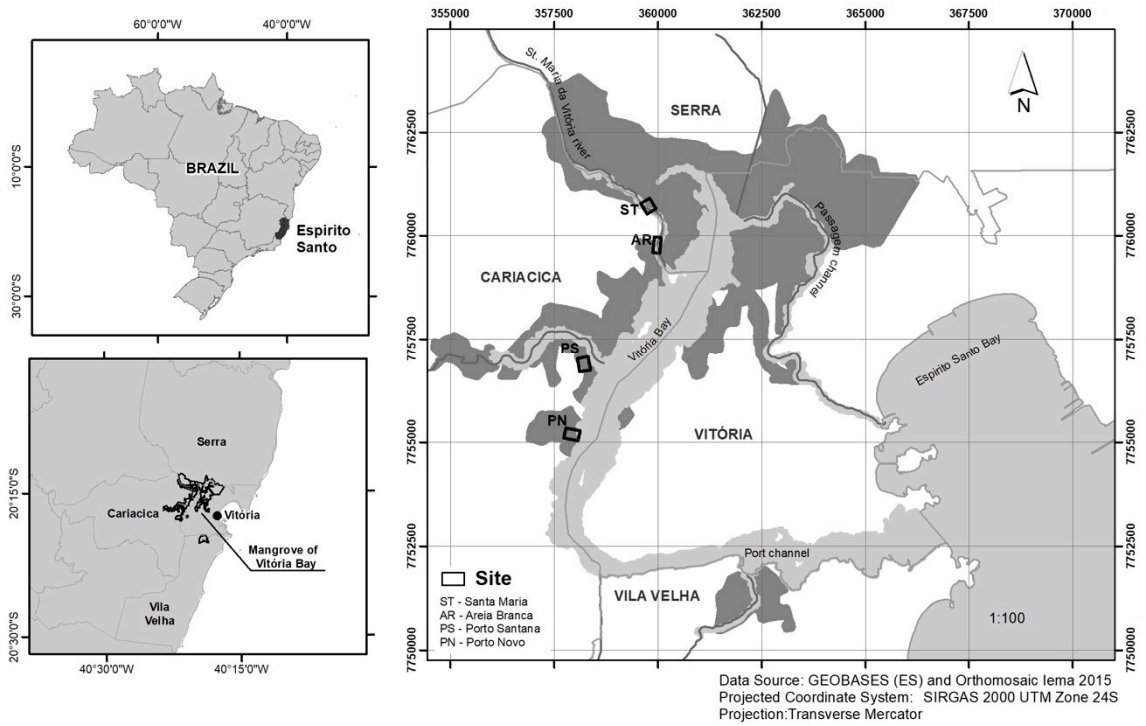

Figure 1. Location of the mangrove of the Vitória Bay, Espírito Santo State, Southeastern Brazil, and the four study areas.

The UAV used was an X700 hexacopter measuring 1.05 m x 0.72 m and weighing 3 kg without battery and gimbal. The battery (LIPO 5200mah to 6000mah 4S Tattu) allows autonomy of 13' of flight. The UAV was equipped with a Tetracam ADC Snap multispectral camera (Tetracam, Inc., Gainesville, USA) weighing 90 g. This camera has three channels with a Charge Coupled Device (CCD) resolution of 1,280 x 1,024 pixels, 10-bit radiometric resolution, 5-micron pixel size, and 8.43 mm focal length. The aperture was set at f/3.2, with 110% exposure time and y~ 2'' capture time. Tetracam ADC Snap is a non-metric, small format camera with green, red, and near-infrared (520 nm – 920 nm).

LAI was obtained using the LAI 2000 Plant Canopy Analyzer (LI-COR, Inc., Lincoln, USA). LAI measurements were performed on cloudy days so that the data were not overestimated, with five

 doi:10.20944/preprints201810.0617.v1

measurements per plot. Measurements were performed in zigzags takes along the transverse line of the plots. Subsequently, mean measurements for each plot were calculated. Structural data of the forest were collected from June 2016 to July 2016 for each of the study areas. Tree height was obtained using a Vertex Laser apparatus (Haglöf, Inc., Madison, USA), and the diameter with a calibrated Forestry Suppliers Metric Fabric diameter tape, model 283D/10M (Forestry Suppliers, Inc., Jackson, USA), thus producing direct readings instead of circumference data. Each study area included eight plots of 10 m x 10 m, totaling 32 plots, which were used to evaluate the different structures representing the forest canopy. The methodology used to obtain and analyze structural data was described by Schaeffer-Novelli and Cintron [26]. The coordinates of the plot vertices were measured with a GNSS Trimble® R4 (Trimble Inc., California, USA) to prepare a georeferenced shapefile in a Geographic Information System.

Shorter and individual flights over each area were planned, considering the autonomy time of the equipment flight and the distribution of study areas. The flight plan was prepared using the free software Mission Planner v 1.3.41 [27]. The flights were executed in October 2016. Geometric rectification was performed with a block adjustment using information on exterior orientation collected during flight with a Global Positioning and Inertial Navigation System (GPS/INS) instrumentation and GPS measurements with ground control points (GCPs). GCPs were measured using a pair of Trimble brand RTK4 GNSS signal receivers, configured with 15° elevation mask and 1'' recording rate. The screening method used was the rapid static, with an occupation time of y~ 5'. The base receiver received real-time corrections from the coordinates database of the Brazilian Institute of Geography and Statistics ("Instituto Brasileiro de Geografia e Estatística"- [28]) through telephone signal. The data were processed in Datum SIRGAS 2000 using the UTM projection system, zone 24, -39º central meridian. Data were downloaded to the Trimble Business Center software [29] and exported to a Microsoft Excel© spreadsheet. The ellipsoidal height was transformed to orthometric altitudes by calculating the geoid undulation in the free software Mapgeo 2015 v 1.0 [28].

Orthomosaic maps were generated for each band separately in the Agisoft Photoscan Professional v 1.2.4 [30]. This software performs internal orientation, automated correspondence between all overlapping images, and simultaneous bundle block adjustment; besides, it produces Digital Surface Models (DSM), Digital Terrain Models (DTM), and orthomosaics. User interventions are necessary to define some parameters such as the correspondence processing method, density of DTM points, and the size of the smallest element in the terrain [30].

The radiometric calibration process was based on converting the DN of the images into a reflectance factor. The spectral characterization of the calibration target (reference surface) was obtained using a FieldSpec Pro model spectroradiometer (Analytical Spectral Devices, Inc., Longmont, USA). This is a portable instrument that can capture spectral data from 350 nm to 2500 nm with a spectral resolution of 1 nm.

An E.V.A. (ethyl vinyl acetate) plate was used as the absolute reference standard because this material shows uniform reflectance to the wavelengths of the used sensors, highly similar to the spectral behavior of a Spectralon plate. During data acquisition, the pistol of the spectroradiometer formed an orthogonal incidence angle with the E.V.A. plate. Three spectral measurements were taken, one at the beginning, one during, and one at the end of the flight.

The reflectance of the reference plate was calculated by weighting the spectral response of the mean radiometric measurements on the plate to the narrow bands 560 nm (B1), 660 nm (B2), and 830 nm (B3), with a Full-Width at Half Maximum (FWHM) of 10 nm. The spectral sensitivity function of the sensor, known as Spectral Response Function (SRF), can be simulated in the form of a Gaussian function, corresponding to the maximum efficiency of the sensor in a given band. SRF can be calculated using the spectral response of the target [31].

The DN conversion of each component, B1, B2, and B3, into the reflectance factor, was performed separately using Matlab v. R2015b [32] image processing environment based on the equation suggested by Miura and Huete [33], as follows:

Preprints (www.preprints.org) | NOT PEER-REVIEWED | Posted: 26 October 2018 doi:10.20944/preprints201810.0617.v1

$$R = \frac{DNt(te)}{DNr(t1)} * Rr,$$

where DNt is the DN of the image reference plate; DNr is the DN of the image where the reference plate is located, and Rr is the reflectance factor of the reference plate measured with the spectroradiometer during flight.

The *RapidEye* Analytic Orthoimage is a multispectral, orthorectified image provided by Planet© [34]. The image was acquired on October 8, 2016, at 13:23 h (UTC) at nadir. The radiometric calibration process was performed in ENVI v 5.1 using the *Fast Line-of-sight Atmospheric Analysis of Hypercubes* (FLAASH algorithm) [35]. All bands were transformed from DN to radiance measurements at the top of the atmosphere, and later to reflectance values. This conversion is only possible for scenes with metadata files (MTL), allowing the process of the following equation [35]:

$$L\lambda = Gain * pixel\ DN + offset.$$

The raster calculator available at ArcGIS Desktop v 10.1 [36] was used to perform arithmetic operations between the spectral bands and to generate the NDVI and SAVI spectral indices of both the UAV and *Rapideye* images. Then, in this same software, *shapefiles* of the plot polygons (10 m x 10 m) were created from coordinate points measured in the field with a *Trimble* RTK4 GPS. The images of the spectral indices were cut using the *shapefiles*, and the mean values of these indices were determined for each plot.

The relationships between the dependent variables LAI, tree height, density of individuals, and DBH obtained *in situ* and the independent variables NDVI and SAVI calculated based on the images were tested, one by one. The regression analysis required success in both the F-test and the T-test to determine the regression modeling result. The modeling method of simple linear regression was used in the regression analysis. The accuracy value of the regression model was obtained by calculating the standard errors of the estimated value. This error can be converted to minimum and maximum precisions with 95% confidence level. The maximum precision value was used to compare the precision of each model.

3. Results

NDVI and SAVI maps were elaborated for four sites in the mangrove. In each site, eight plots were established in the field, totaling 32 plots. In the processing of aerial photos obtained by UAV, there were some problems, and five plots did not have the aerial overlay. In the NDVI map, the mangrove clearings showed high index values due to the wet soil and organic matter content. In the SAVI map, the 0.5 adjustment factor was used, and a better result was obtained when compared to the NDVI map. It was possible to separate the clearings from the canopy, and the index values for *L. racemosa* were lower than for *R. mangle*, allowing species discrimination and identification of the succession pattern (Figure 2).

Preprints (www.preprints.org) | NOT PEER-REVIEWED | Posted: 26 October 2018 doi:10.20944/preprints201810.0617.v1

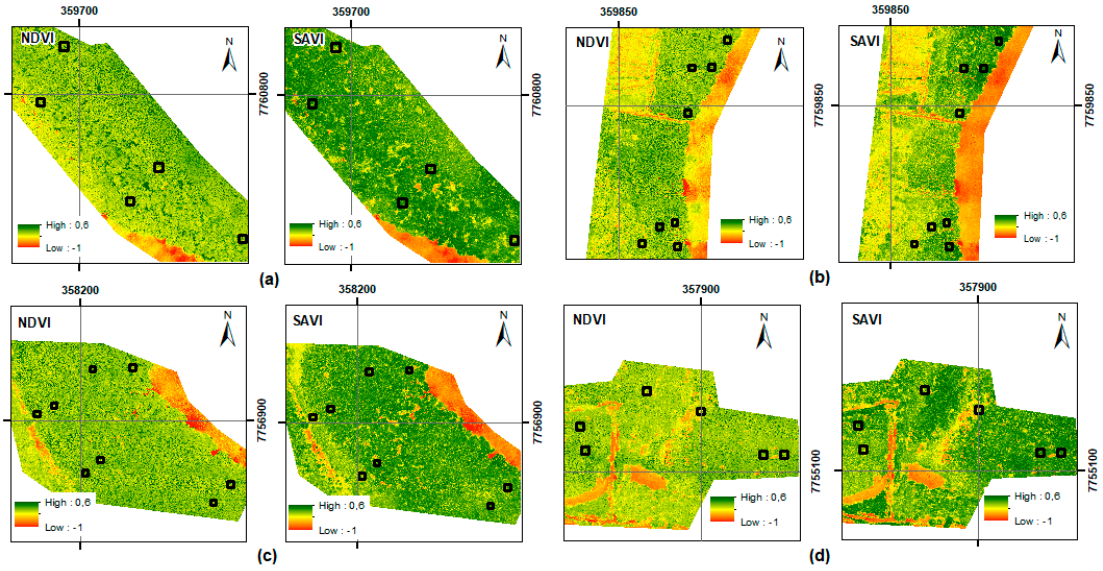

Figure 2. NDVI and SAVI images of the four study areas from the urban mangrove of the Vitória Bay, Espírito Santo State, Southeastern Brazil: (**a**) Santa Maria; (**b**) Areia Branca; (**c**) Porto Santana; and (**d**) Porto Novo.

The structural data collected in the field and the spectral indices obtained from the orthomosaic and *Rapideye* images are in Table 1. The plot structure data were converted into estimates of basal area dominance per plot (Figure 3), *i.e.*, the soil area occupied by individual biomass. *Rhizophora mangle* was dominant in most of the plots, particularly in Santa Maria; on the other hand, *L. racemosa* was dominant only in eight plots.

Table 1. Structure and spectral data of the study stations in the urban mangrove of the Vitória Bay, Espírito Santo State, Southeastern Brazil. RZ, *Rhizophora mangle;* LAG, *Laguncularia racemosa;* LAI, Leaf Area Index; DBH, Diameter at Breast Height; Fr, Fringe mangrove; B, Basin mangrove; H, height.

Site	Species	Plot ID	Field LAI (m2/m2)	Absolute tree density/ 0.1 ha	Mean DBH	trunk/ tree	Type	H (m)	NDVI*	SAVI*	*NDVI***	*SAVI***
Porto Novo	RZ	101	1.97	4.6	7.8	1.1	Fr	4.57	0.54	0.45	0.84	0.49
Porto Novo	RZ	102	2.24	2.4	7.48	1.0	Fr	5.19	0.54	0.43	0.82	0.46
Porto Novo	LAG	10	2.06	7.9	5.02	1.15	B	6.21	0.55	0.34	0.73	0.35
Porto Novo	LAG	11	2.27	5.1	9.32	1.1	B	10.7	0.56	0.36	0.79	0.41
Porto Novo	LAG	2	1.82	5.7	5.91	1.2	B	5.07	0.49	0.34	0.6	0.3
Porto Novo	RZ	3	0.85	800	12.24	1.5	B	6.98	0.42	0.28	0.6	0.3
Porto	LAG	3	0.96	3.5	9.98	1.0	B	9.07	0.57	0.29	0.6	0.3

 doi:10.20944/preprints201810.0617.v1

Santana												
Porto Santana	RZ	4	1.68	1.2	15.7	1.0	B	13.47	0.59	0.38	0.82	0.45
Porto Santana	LAG	5	1.48	5.4	8.21	1.0	B	13.08	0.63	0.33	0.76	0.34
Porto Santana	RZ	7	2.22	2.4	8.33	1.1	B	15.13	0.59	0.41	0.87	0.5
Porto Santana	RZ	100	1.82	7.3	5.96	1.0	Fr	4.4	0.59	0.40	0.82	0.49
Porto Santana	RZ	2	1.49	2.6	12.42	1.0	B	8.16	0.61	0.36	0.79	0.44
Porto Santana	RZ	3	2.61	900	22.66	2	Fr	18.6	0.59	0.42	0.84	0.53
Porto Santana	RZ	4	3.93	9.8	3.88	1	B	5.41	0.64	0.40	0.84	0.47
Areia Branca	LAG	1	1.57	6.1	10.19	1.3	Fr	9.73	0.66	0.32	0.77	0.37
Areia Branca	RZ	6	2.36	2.2	12.28	2.7	B	10.55	0.60	0.36	0.87	0.47
Areia Branca	RZ	5	2.88	3	7.68	1.1	Fr	4.95	0.62	0.41	0.88	0.49
Areia Branca	RZ	7	2.26	1.1	17.42	1.3	Fr	12.1	0.57	0.43	0.84	0.50
Areia Branca	RZ	9	1.92	1.3	9.51	1.3	Fr	8.5	0.62	0.33	0.85	0.46
Areia Branca	LAG	11	2.12	6.5	5.43	1.3	B	5.22	0.63	0.28	0.72	0.31
Areia Branca	LAG	1000	1.65	7.2	5.26	1.5	B	4.07	0.56	0.28	0.61	0.25
Areia Branca	RZ	20	2.77	1.5	13.29	1.3	Fr	13.13	0.57	0.40	0.85	0.49
Santa Maria	RZ	2	2.39	2.2	9.69	1.3	Fr	6	0.63	0.37	0.85	0.48
Santa Maria	RZ	3	3.03	3.2	11.28	1.2	B	6.56	0.56	0.45	0.86	0.47
Santa Maria	RZ	30	2.33	1	15.15	1.3	Fr	9.92	0.59	0.45	0.85	0.51
Santa Maria	RZ	31	2.42	1.8	15.6	2.2	B	10.98	0.61	0.41	0.87	0.50
Santa Maria	RZ	20	2.03	1.8	12.31	1.4	B	11.68	0.61	0.33	0.84	0.45

234 * **VANT;** ***RapidEye***
235
236

 doi:10.20944/preprints201810.0617.v1

Forest density was negatively correlated with mean DBH (r=-0.78; p <0.05; Spearman's test). These results are in line with the assumption that the density is reduced in more mature forests when the mean DBH value becomes higher [26]. Few trees of larger diameters characterize these forests.

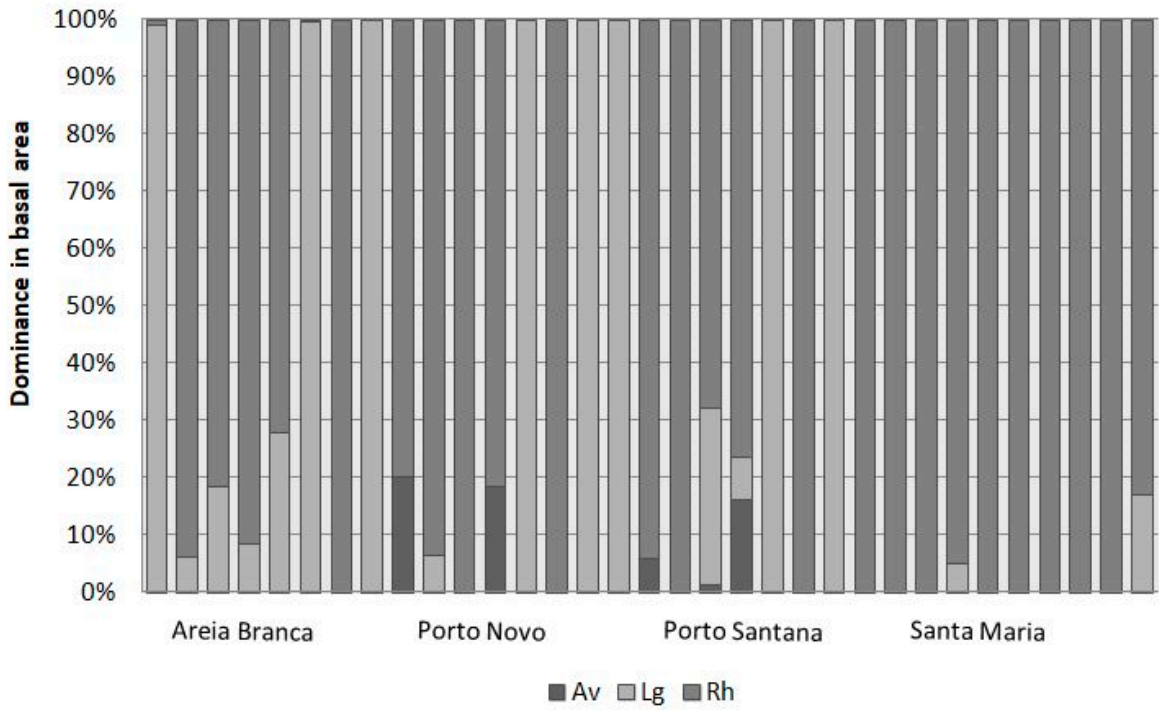

Figure 3. The dominance of individuals of *Avicennia schaueriana* (Av), *Laguncularia racemosa* (Lg), and *Rhizophora mangle* (Rh) in the four study areas from the urban mangrove of the Vitória Bay, Espírito Santo State, Southeastern Brazil.

Figure 4 shows a chart of the height and mean diameter of the plots measured in the field for each study area. It is possible to observe the structural variability between them. Concerning the LAI, the mean value was 2.08 for the plots analyzed, 2.25 for *R. mangle*, and 1.74 for *L. racemosa*. It is worth mentioning that, although the measurements were carried out in October, a typical rainy month in Southeastern Brazil, October 2016 was an atypical month with precipitation values of 125 mm and evapotranspiration of 17 mm [37].

Preprints (www.preprints.org) | NOT PEER-REVIEWED | Posted: 26 October 2018 doi:10.20944/preprints201810.0617.v1

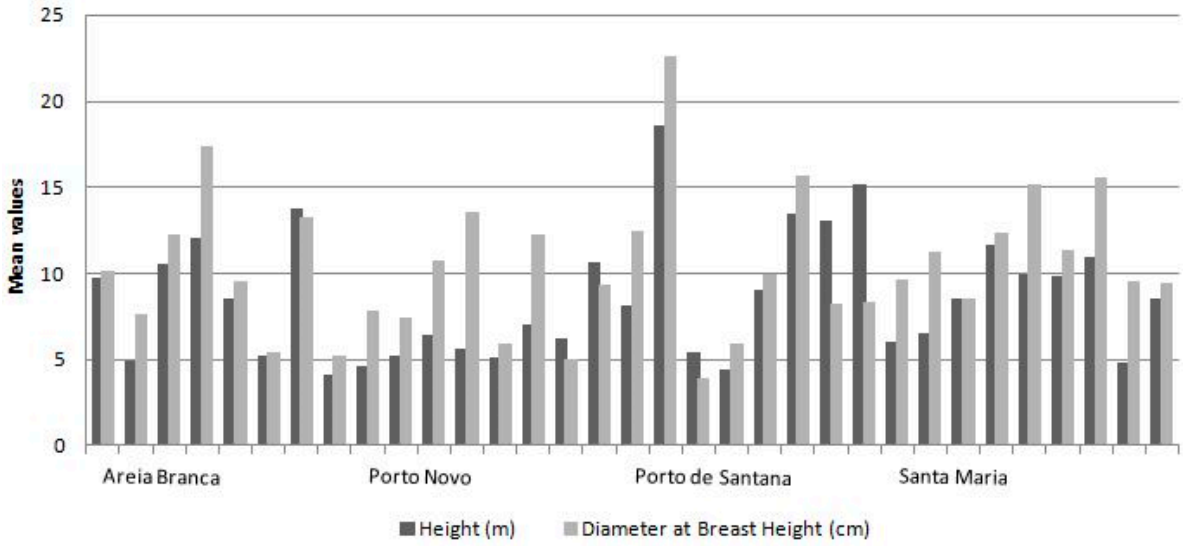

Figure 4. Mean values of tree height (m) and mean diameter (cm) for each plot in the study areas in the urban mangrove of the Vitória Bay, Espírito Santo State, Southeastern Brazil.

Correlation analysis led to the identification of LAI as the only dependent variable that was a candidate for regression since the others (tree height, density of individuals, and DBH) were not significantly correlated with the independent variables NDVI and SAVI. The highest value was obtained for the regression of the variable LAI x SAVI (r^2 = 43%) with a significant coefficient since when analyzing the statistical significance of the *Student's* t-test, the null hypothesis of non-significance was rejected (*p-value* <0.05).

Table 2 shows that the regression analysis of the *in situ* LAI variable with NDVI and SAVI resulted in significant positive relationships, with SAVI presenting the best result. When analyzing only the plots 100% dominated by *R. mangle* or *L. racemosa*, the r^2 of LAI x SAVI increased to 0.53. In the analysis of the data using only the *R. mangle* plots, the r^2 values were 0.58 for SAVI.

Table 2. The coefficient of determination (r^2) of the regression of the leaf area index (LAI) dependent variable and the independent variables NDVI and SAVI, using Unmanned Aerial Vehicle (UAV) and *Rapideye* images.

Dependent variable	Statistics	Independent variables		Species dominance in plots	Images
		NDVI (r^2)	SAVI (r^2)		
LAI	r^2	0.23	0.43	> 90% (*L. racemosa* and *R. mangle*)	UAV
	p-value (α)	0.01	0.00		
LAI	r^2	0.07	0.53	100% (*L. racemosa* and *R. mangle*)	
	p-value (α)	0.22	0.00		
LAI	r^2	0.36	0.58	only *R. mangle*	
	p-value (α)	0.06	0.01		
LAI	r^2	0.7	0.7	only *R. mangle*	*Rapideye*
	p-value (α)	0.002	0.003		

Preprints (www.preprints.org) | NOT PEER-REVIEWED | Posted: 26 October 2018 doi:10.20944/preprints201810.0617.v1

Figure 5 shows the reflectance image (*RapidEye*) with RGB 532 composition. Bands 5 (NIR) and 3 (RED) were used to elaborate NDVI and SAVI maps.

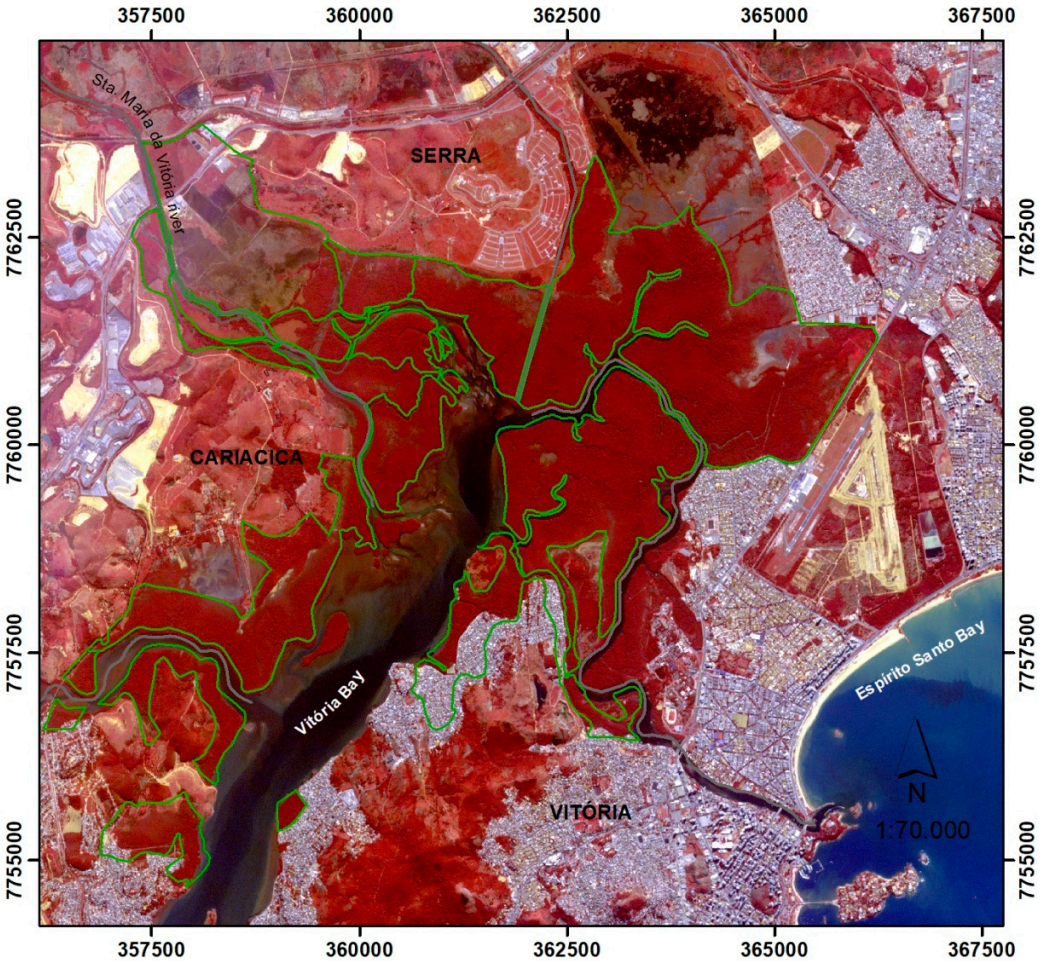

Figure 5. Reflectance image (*RapidEye*) with RGB 532 composition.

Figure 6 shows the difference between the two sensors regarding spatial resolution. The Tetracam ADC *Snap* sensor has the pixel size of 5 mm, whereas the *RapidEye* sensor has the pixel size of 5 m. There are also differences in spectral resolution. The Tetracam ADC *Snap* camera sensor displays the RED and NIR bands centered at 660 nm and 830 nm, respectively, and the spectral resolution of the FWHM is 10 nm. The *RapidEye* satellite has the RED and NIR bands centered at 660 nm (FWHM = 60 nm) and 820 nm (FWHM = 120 nm), respectively.

Preprints (www.preprints.org) | NOT PEER-REVIEWED | Posted: 26 October 2018 doi:10.20944/preprints201810.0617.v1

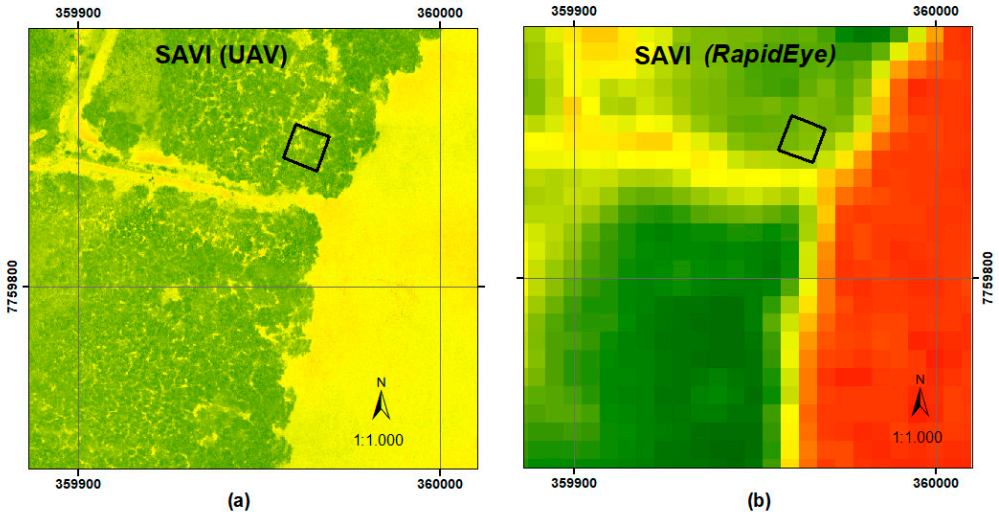

Figure 6. Images of the vegetation index SAVI; (**a**) Tetracam ADC *Snap* sensor; (**b**) *RapidEye* satellite.

Figure 7 shows the SRF of the two sensors and the spectral behavior of the mangrove. The *RapidEye* satellite has the *RedEdge* band between 690 nm and 730 nm, which is very useful for vegetation monitoring. However, it was not used in this research because our goal was to work with the same Tetracam sensor bands.

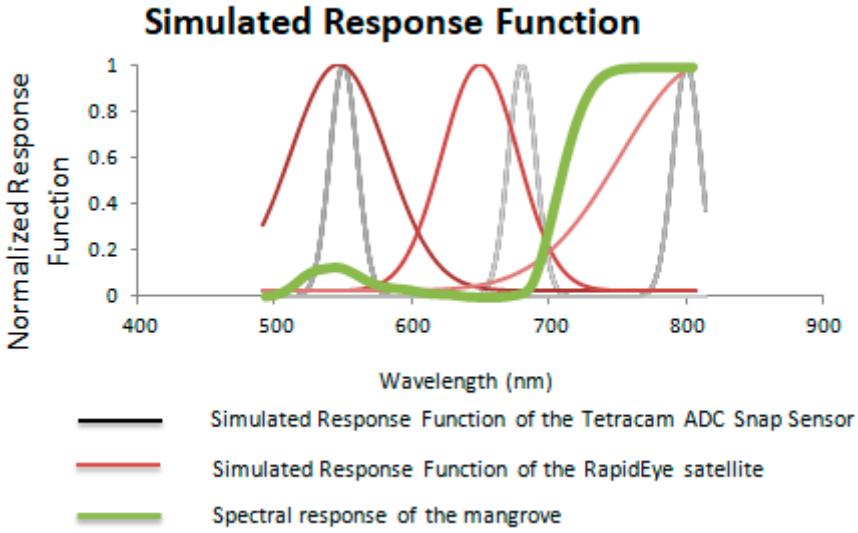

Figure 7. Spectral Response Function of the Tetracam ADC *Snap* and *RapidEye* sensors together with the spectral response of the mangrove.

The same data collected in the field were correlated with NDVI and SAVI from a *RapidEye* image. The data were significant in the regression analysis; the LAI x NDVI and LAI x SAVI r^2 were 0.7.

 doi:10.20944/preprints201810.0617.v1

4. Discussion

The Santa Maria forests had lower density values in comparison to the other areas; they are more structurally developed (Figure 4) and characterized by monospecific forests of *R. mangle*. The stations defined in this study are located in more muddy areas and further away from urban occupation. The VIs values were higher than the mean values of the other studied areas.

The mangrove in Porto Novo suffers strong anthropogenic pressure [38], as raw sewage and landfills can be seen in the mangroves. Porto Novo had the highest diversity value of forest structure. This explains the highest variability of the NDVI data from the orthomosaics. This forest, as a whole, is undergoing changes in its structure, which become more evident when data from the plot 3 (Table 1) were analyzed, with few individuals of larger size (DBH> 15 cm) and a massive presence of juveniles. These characteristics are reflected in the *in situ* data for *R. mangle*, with LAI values below the mean and lower VIs values.

In Porto Santana, the L4 plot with a dominance of *R. mangle* had the highest density values, but presented the smallest mean diameter values as a clearing being colonized by young individuals was observed. Besides, the plots with the highest density values were dominated by *L. racemosa*. The L3 plot, dominated by *R. mangle*, had the highest values of tree height and DBH. This forest is located in the mangrove fringe and has maintenance of large live trees. When comparing the VIs, although the data of this area were close to those of Areia Branca, they did not differ significantly from the other areas. This occurs because the forest of Porto Santana has a high structural variability, exclusive of the forests dominated by *R. mangle*. The forest dominated by *L. racemosa* had structure patterns similar to the overall average of the region, reflecting in the VIs data, which were highly similar to those of *R. mangle* forests.

When evaluating the forest structure regarding the distribution of individuals by diameter classes, it was possible to verify that the forests of Areia Branca showed intermediate stages with similar characteristics to the forests of Porto Santana. The mean values of LAI found for the *R. mangle* and *L. racemosa* (2.25 and 1.74, respectively) were similar to those found in previous studies. When compared to the sub-forests of tropical forests, mangroves tend to present lower values of field-measured LAI [24]. Studies in Puerto Rico and Southeast Florida (USA) found LAI values for *R. mangle* of 4.4 and 3.5, respectively. Kovacs et al. [25] found a LAI value of 2.49 for *R. mangle* and 1.74 for *L. racemosa* in mature forests, and 0.85 for *L. racemosa* in some plots in mangroves in Mexico. Flores-de-Santiago et al. [39] performed LAI measurements in a rainy and a dry season in a mangrove forest in the Mexican Pacific. In their study, LAI values for *R. mangle* characterized as poor mangrove ranged, from the rainy to the dry season, between 2.1 and 2.4.

On the other hand, the values of healthy *R. mangl*e were between 5.7 and 5.1. For *L. racemosa* characterized as poor, the range was between 1.4 and 1.2; for the same healthy species, between 2.5 and 3.6. The species *A. germinans*, characterized as dwarf mangrove, did not vary from one period to another, with LAI = 1.5. In plots with this same species characterized as healthy, the values were from 3.6 to 2.9. Lima [40] studied a mangrove area dominated by *R. mangle* in Barra do Ribeira, Brazil, and observed LAI values for this species of 1.18 and 0.96 in the rainy and dry seasons, respectively. The author proposed an increase in leaf production by reduction of interstitial salinity, favoring the formation of new leaves in the rainy season.

Concerning the correlation analysis, the highest value of the r^2 was 0.7 between the dependent variable LAI and the independent variable SAVI. This analysis considered only the data of IAF and SAVI of *R. mangle*. The results show that, even for the satellite images with a high geometric and radiometric quality, the correlation analysis did not present a high value of r^2. With respect to the data of the UAV images, the correlation analysis between the dependent variable IAF and the independent variable SAVI had $r^2 = 0.58$. This suggests that the UAV images suffer a more significant influence of the soil due to the higher spatial resolution.

Gao [41] stated that the influence of the soil surface is higher in mangrove plots with a lower density of individuals and sparse treetops. Diaz and Blackburn [8] suggested that the spectral variations related to the reflectance of the mangrove canopy are due to variables including LAI, substrate characteristics, and leaf inclination angle. The differences in mangrove structure and LAI

 doi:10.20944/preprints201810.0617.v1

values between *R. mangle* and *L. racemosa* were variables that influenced the adjustment of VIs with field data in this study.

Positive regression analysis indicated that the higher the SAVI, the higher the LAI. Besides, the higher the LAI, the better the distribution of canopy height in the forest; furthermore, greater overlap of leaves influenced less the substrate in the spectral data. The density values were smaller in the plots of *R. mangle*, but these were more structurally developed and had higher LAI values when compared to the plots of *L. racemosa*. The higher coverage of the soil by litterfall and the higher number of young individuals measuring less than 50 cm in height, not counted in the statistics, may have contributed to minimize the bottom soil effect, and consequently improve the LAI adjustment with the SAVI in the homogeneous plots of *R. mangle*.

5. Conclusions

The high spatial resolution of the orthophotos obtained by UAV allows several analyzes of the mangrove using photo interpretation. These include vegetation distribution analysis, structural differences between *R. mangle* and *L. racemosa*, identification of dominant species, succession patterns, and clearing mapping. Regarding the use of reflectance images and their derivatives, more detailed studies on the influences of biological (*e.g.*, LAI, substrate characteristics, and leaf inclination angle) and environmental (*e.g.*, salinity and tidal flood patterns) variables are still needed.

The sensor coupled to the UAV needs to be evaluated concerning the spectral band sensitivity and its SRF. Regarding the radiometric calibration of aerial photos, the BRDF needs to be considered in future works due to variations of the θv. A critical issue in creating the BRDF is that it should be done in the field, and this can be complicated since the object of study is the mangrove.

The NDVI map did not show a satisfactory result since the mangrove clearings had high index values due to the wet soil. The SAVI map rendered a better outcome for species differentiation and clearing identification. The SAVI values for *L. racemosa* were lower than for *R. mangle*, allowing species discrimination and identification of the succession pattern.

The correlation between the dependent variable LAI (*in situ*) and the independent variable SAVI had the r^2 increased from 0.43 to 0.53 when the field data of the plots with 100% dominance of *R. mangle* or *L. racemosa* were used. When only the *R. mangle* field data of the LAI versus SAVI variables were correlated, r^2 increased to 0.58.

The plots of *L. racemosa* showed higher density and lower LAI values, as well as greater variability in the structure data. The lower LAI values contributed to increasing the influence of the substrate on the spectral response of the sensor. The higher structural development of *R. mangle* forests, their higher LAI value, and more homogeneous forests contributed to the better adjustment of the data.

The IVs extracted from the UAV images, and the LAI data collected in the field presented low r^2 values, partly due to the high structural variability of the studied stations, mainly concerning *L. racemosa*. The mangrove forests of the Vitória Bay are subject to different human-induced environmental tensors, such as landfills and raw sewage. This can also interfere with the homogeneity of the structural data, and consequently with the spectral data. Besides, the different compositions of the mangrove soil, the rate of soil cover per litter, the tidal flood pattern, the interstitial salinity, and even atmospheric pollution (e.g., particulates of iron ore deposited under the leaf) need to be considered in future studies, as they may interfere with the reflectance of the canopy.

Concerning the *Rapideye* image, the correlation between LAI (*in situ*) and NDVI (*RapidEye*) and LAI (*in situ*) x SAVI (*RapidEye*) presented an r^2 of 0.7. This shows that, even when satellite images with a high degree of geometric and radiometric quality were used, the correlation analysis did not show a high r^2 value. The use of IVs for monitoring anthropogenically influenced mangroves and heterogeneous structural forests is still challenging.

If on the one hand, the orbital images have a high degree of geometric and spectral quality, on the other the images obtained by UAV have a very high spatial resolution; in addition, the time of

418 revisiting the studied object can be defined according to the interest of the researcher, for example, at
419 low tides. Thus, images obtained by UAV are useful tools of coastal management and monitoring of
420 the mangrove ecosystem; however, greater care is required when capturing spectral images. This
421 type of image requires an appropriate sensor and a radiometric calibration process based on a
422 Bidirectional Reflectance Factor model.
423

424 **Author Contributions:** "conceptualization, Silva and Tognella; methodology, Silva, Tognella, Xavier and
425 Tedesco; validation, Silva, Tognella and Xavier; investigation, Silva; resources, Silva, Tognella, Xavier, Tedesco,
426 Neto, Pezzopane and Lima; writing—original draft preparation, Silva; writing—review and editing, Tognella,
427 Xavier, Tedesco, Neto, Pezzopane and Lima; supervision, Tognella."

428 **Funding:** "This research was partially funded by the Coordenação de Aperfeiçoamento de Pessoal de Nível
429 Superior (CAPES), Brazil - Finance Code 001. Tognella was supported by Fundação de Amparo à Pesquisa e
430 Inovação do Espírito Santo (FAPES), research budget No. 385, grants No. 60127627/2012 and 263/2016).

431 **Acknowledgments:** In this section you can acknowledge any support given which is not covered by the author
432 contribution or funding sections. This may include administrative and technical support, or donations in kind
433 (e.g., materials used for experiments). The authors are grateful to the Education and Research Program of the
434 Planet© Company for providing the *Rapideye* image. We also thank the *Fundo Brasileiro para Biodiversidade*
435 (FUN-BIO) for providing the Tetracam, TFCA Agreement N°04/2012, and CAPES (ProPos 2013) for providing
436 the RTK-4. M.

437 **Conflicts of Interest:** "The authors declare no conflict of interest. The funders had no role in the design of the
438 study; in the collection, analyses, or interpretation of data; in the writing of the manuscript, or in the decision to
439 publish the results".
440

References

1. Daughtry, C.S.T.; Walthall, C.L.; Kim, M.S.; de Colstoun, E.B.; McMurtrey III, J.E. Estimating Corn Leaf Chlorophyll Concentration from Leaf and Canopy Reflectance. *Remote Sens. Environ.* **2000**, *74*, 229–239, doi:http://dx.doi.org/10.1016/S0034-4257(00)00113-9.

2. Haboudane, D.; Miller, J.R.; Pattey, E.; Zarco-Tejada, P.J.; Strachan, I.B. Hyperspectral vegetation indices and novel algorithms for predicting green LAI of crop canopies: Modeling and validation in the context of precision agriculture. *Remote Sens. Environ.* **2004**, *90*, 337–352, doi:https://doi.org/10.1016/j.rse.2003.12.013.

3. Green, E.P.; Clark, C.D.; Mumby, P.J.; Edwards, A.J.; Ellis, A.C. Remote sensing techniques for mangrove mapping. *Int. J. Remote Sens.* **1998**, *19*, 935–956, doi:10.1080/014311698215801.

4. Kovacs, J.M.; Flores-Verdugo, F.; Wang, J.; Aspden, L.P. Estimating leaf area index of a degraded mangrove forest using high spatial resolution satellite data. *Aquat. Bot.* **2004**, *80*, 13–22, doi:https://doi.org/10.1016/j.aquabot.2004.06.001.

5. Wang, L.; Sousa, W.P.; Gong, P.; Biging, G.S. Comparison of IKONOS and QuickBird images for mapping mangrove species on the Caribbean coast of Panama. *Remote Sens. Environ.* **2004**, *91*, 432–440, doi:https://doi.org/10.1016/j.rse.2004.04.005.

6. Proisy, C.; Couteron, P.; Fromard, F. Predicting and mapping mangrove biomass from canopy grain analysis using Fourier-based textural ordination of IKONOS images. *Remote Sens. Environ.* **2007**, *109*, 379–392, doi:https://doi.org/10.1016/j.rse.2007.01.009.

7. Vaiphasa, C.; Ongsomwang, S.; Vaiphasa, T.; Skidmore, A.K. Tropical mangrove species discrimination using hyperspectral data: A laboratory study. *Estuar. Coast. Shelf Sci.* **2005**, *65*, 371–379, doi:https://doi.org/10.1016/j.ecss.2005.06.014.

8. Díaz, B.M.; Blackburn, G.A. Remote sensing of mangrove biophysical properties: Evidence from a laboratory simulation of the possible effects of background variation on spectral vegetation indices. *Int. J. Remote Sens.* **2003**, *24*, 53–73, doi:10.1080/01431160305012.

9. Jones, J.; Dale, P.E.R.; Chandica, A.L.; Breitfuss, M.J. Changes in the distribution of the grey mangrove Avicennia marina (Forsk.) using large scale aerial color infrared photographs: are the changes related to habitat modification for mosquito control? *Estuar. Coast. Shelf Sci.* **2004**, *61*, 45–54, doi:https://doi.org/10.1016/j.ecss.2004.04.002.

10. Dahdouh-Guebas, F.; Van Pottelbergh, I.; Kairo, J.G.; Cannicci, S.; Koedam, N. Human-impacted mangroves in Gazi (Kenya): Predicting future vegetation based on retrospective remote sensing, social surveys, and tree distribution. *Mar. Ecol. Prog. Ser.* **2004**, *272*, 77–92, doi:10.3354/meps272077.

11. Ponzoni, F.J.; Shimabukuro, Y.E.; Kuplich, T.M. *Sensoriamento Remoto no Estudo da Vegetação*; 2nd.; Oficina de Textos: São Paulo, 2012; ISBN 978-85-7975-053-3.

12. Kollenkark, J.C.; Vanderbilt, V.C.; Daughtry, C.S.T.; Bauer, M.E. Influence of solar illumination angle on soybean canopy reflectance. *Appl. Opt.* **1982**, *21*, 1179–1184, doi:10.1364/AO.21.001179.

13. Huete, A.R. A soil-adjusted vegetation index (SAVI). *Remote Sens. Environ.* **1988**, *25*, 295–309, doi:https://doi.org/10.1016/0034-4257(88)90106-X.

14. Rouse, J. W., J.; Haas, R.H.; Schell, J.A.; Deering, D.W. Monitoring vegetation systems in the Great Plains with ERTS. In; Texas A&M Univ.; College Station, TX, United States: Texas, 1974; pp. 309–317.

15. Baret, F.; Guyot, G.; Major, D. *TSAVI: A vegetation index which minimizes soil brightness effects on LAI and APAR estimation*; 1989; Vol. 3;.

16. Baret, F.; Guyot, G. Potentials and limits of vegetation indices for LAI and APAR assessment. *Remote Sens. Environ.* **1991**, *35*, 161–173, doi:10.1016/0034-4257(91)90009-U.

17. Qi, J.; Chehbouni, A.; Huete, A.R.; Kerr, Y.H.; Sorooshian, S. A modified soil adjusted vegetation index. *Remote Sens. Environ.* **1994**, *48*, 119–126, doi:https://doi.org/10.1016/0034-4257(94)90134-1.

18. Rondeaux, G.; Steven, M.; Baret, F. Optimization of soil-adjusted vegetation indices. *Remote Sens. Environ.* **1996**, *55*, 95–107, doi:https://doi.org/10.1016/0034-4257(95)00186-7.

19. Zhang, C.; Liu, Y.; Kovacs, J.M.; Flores-Verdugo, F.; Santiago, F.F. de; Chen, K. Spectral response to varying levels of leaf pigments collected from a degraded mangrove forest. *J. Appl. Remote Sens.* **2012**, *6*, 063501-1-063501-14, doi:10.1117/1.JRS.6.063501.

20. Hakala, T.; Honkavaara, E.; Saari, H.; Mäkynen, J.; Kaivosoja, J.; Pesonen, L.; Pölönen, I. *Spectral imaging from UAVs under varying illumination conditions*; 2013; Vol. XL-1/W2;

21. Schaepman-Strub, G.; Schaepman, M.E.; Painter, T.H.; Dangel, S.; Martonchik, J. V Reflectance quantities in optical remote sensing—definitions and case studies. *Remote Sens. Environ.* **2006**, *103*, 27–42, doi:https://doi.org/10.1016/j.rse.2006.03.002.

22. Honkavaara, E.; Saari, H.; Kaivosoja, J.; Pölönen, I.; Hakala, T.; Litkey, P.; Mäkynen, J.; Pesonen, L. Processing and Assessment of Spectrometric, Stereoscopic Imagery Collected Using a Lightweight UAV Spectral Camera for Precision Agriculture. *Remote Sens.* 2013, *5*.

23. Koukal, T.; Schneider, W. Analysis of Brdf Characteristics of Forest Stands With a Digital Aerial Frame Camera. In *Symposium A Quarterly Journal In Modern Foreign Literatures*; International Archives of the Photogrammetry, Remote Sensing and Spatial Information Sciences: Vienna, 2010; Vol. XXXVIII, pp. 100–105.

24. Ramsey, E.W.; Jensen, J.R. Remote Sensing of Mangrove Wetlands: Relating Canopy Spectra to Site-Specific Data. *Photogramm. Eng. Remote Sensing* **1996**, *62*, 939–948.

25. Kovacs, J.M.; Wang, J.; Flores-Verdugo, F. Mapping mangrove leaf area index at the species level using IKONOS and LAI-2000 sensors for the Agua Brava Lagoon, Mexican Pacific. *Estuar. Coast. Shelf Sci.* **2005**, *62*, 377–384, doi:10.1016/j.ecss.2004.09.027.

26. Schaeffer-Novelli, Y.; Cintron, G.P.P.-S.P. *Guia para estudo de areas de manguezal. Estrutura, função e flora*; Caribbean Ecological Research: São Paulo, 1986;

27. Team, A.D. Mission Planner Available online: http://firmware.ardupilot.org/Tools/MissionPlanner/archive/.

28. IBGE - Instituto Brasileiro de Geografia e Estatística Available online: https://www.ibge.gov.br/geociencias-novoportal/informacoes-sobre-posicionamento-geodesico/rede-geodesica/16258-rede-brasileira-de-monitoramento-continuo-dos-sistemas-gnss-rbmc.html?=&t=o-que-e (accessed on Jul 20, 2003).

29. Trimble Business Center.

30. Agisoft Agisoft PhotoScan User Manual: Professional Edition, Version 1.4. *Agisoft PhotoScan User Man. Prof. Ed.* 2018, 37.

31. *Spatial Statistics for Remote Sensing*; Stein, A., Van der Meer, F., Gorte, B., Eds.; Remote Sensing and Digital Image Processing; Kluwer Academic Publishers: Verlag, 1999; Vol. 1;.

32. The MathWorks, I. Matlab.

33. Miura, T.; Huete, A. Performance of Three Reflectance Calibration Methods for Airborne Hyperspectral Spectrometer Data. *Sensors* **2009**, *9*, 794–813, doi:10.3390/s90200794.

34. Planet Team *Planet Application Program Interface: In Space for Life on Earth*; San Francisco, 2017;

35. EXELIS Fast Line-of-sight Atmospheric Analysis of Hypercubes (FLAASH) Available online: http://www.exelisvis.com/docs/FLAASH.html (accessed on Nov 7, 2014).

36. Esri ArcGIS Desktop Available online: https://www.esri.com/en-us/arcgis/about-arcgis/overview.

37. Instituto Capixaba de Pesquisa, Assistência Técnica e Extensão Rural Available online: https://meteorologia.incaper.es.gov.br/graficos-da-serie-historica (accessed on Mar 2, 2018).

38. Zamprogno, G.C. Use of biological and environmental factors in the evaluation of vulnerability levels of mangrove forests in the Bay of Vitória, ES, Universidade Federal do Espírito Santo, 2015.

39. Flores-de-Santiago, F.; Kovacs, J.; Wang, J.; Flores-Verdugo, F.; Zhang, C.; González-Farías, F.; Flores-de-Santiago, F.; Kovacs, J.M.; Wang, J.; Flores-Verdugo, F.; Zhang, C.; González-Farías, F. Examining the Influence of Seasonality, Condition, and Species Composition on Mangrove Leaf Pigment Contents and Laboratory Based Spectroscopy Data. *Remote Sens.* **2016**, *8*, 226, doi:10.3390/rs8030226.

40. Lima, N.G.B. de Análise microclimática dos manguezais da Barra do Ribeira-Iguape/SP, Universidade de São Paulo: São Paulo, 2009.

542 41. Gao, J. A comparative study on spatial and spectral resolutions of satellite data in mapping mangrove
543 forests. *Int. J. Remote Sens.* **1999**, *20*, 2823–2833, doi:10.1080/014311699211813.